AD-A154 952 AUTOMATED CELL DETECTION AS A MESOCYCLONE PRECURSOR TOOL(U) SYSTEMS AND APPLIED SCIENCES CORP VIENNA VA F I HARRIS ET AL. 05 OCT 84 AFGL-TR-84-0266 1/1

UNCLASSIFIED F19628-82-C-0023 F/G 4/2 NL

END

FILMED

DTIC

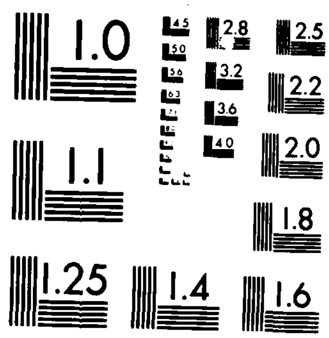

MICROCOPY RESOLUTION TEST CHART
NATIONAL BUREAU OF STANDARDS-1963-A

(2)

AFGL-TR-84-0266
ENVIRONMENTAL RESEARCH PAPERS, NO. 891

AD-A154 952

Automated Cell Detection as a Mesocyclone Precursor Tool

F. IAN HARRIS
PIO J. PETROCCHI

5 October 1984

Approved for public release; distribution unlimited.

ATMOSPHERIC SCIENCES DIVISION PROJECT 6670
AIR FORCE GEOPHYSICS LABORATORY
HANSCOM AFB, MA 01731

This report has been reviewed by the ESD Public Affairs Office (PA) and is releasable to the National Technical Information Service (NTIS).

This technical report has been reviewed and is approved for publication.

FOR THE COMMANDER

Kenneth M Glover

KENNETH M. GLOVER
Chief, Ground Based Remote Sensing Branch
Meteorology Division

Robert A. McClatchey

ROBERT A. MCCLATCHEY
Director, Meteorology Division

Qualified requestors may obtain additional copies from the Defense Technical Information Center. All others should apply to the National Technical Information Service.

If your address has changed, or if you wish to be removed from the mailing list, or if the addressee is no longer employed by your organization, please notify AFGL/DAA, Hanscom AFB, MA 01731. This will assist us in maintaining a current mailing list.

Do not return copies of this report unless contractual obligations or notices on a specific document requires that it be returned.

UNCLASSIFIED

SECURITY CLASSIFICATION OF THIS PAGE

REPORT DOCUMENTATION PAGE

1a. REPORT SECURITY CLASSIFICATION Unclassified	1b. RESTRICTIVE MARKINGS
2a. SECURITY CLASSIFICATION AUTHORITY	3. DISTRIBUTION/AVAILABILITY OF REPORT Approved for public release; distribution unlimited.
2b. DECLASSIFICATION/DOWNGRADING SCHEDULE	
4. PERFORMING ORGANIZATION REPORT NUMBER(S) AFGL-TR-84-0266 ERP, No. 891	5. MONITORING ORGANIZATION REPORT NUMBER(S)
6a. NAME OF PERFORMING ORGANIZATION Air Force Geophysics Laboratory 6b. OFFICE SYMBOL (If applicable) LYR	7a. NAME OF MONITORING ORGANIZATION Air Force Geophysics Laboratory
6c. ADDRESS (City, State and ZIP Code) Hanscom AFB Massachusetts 01731	7b. ADDRESS (City, State and ZIP Code) Hanscom AFB Massachusetts 01731
8a. NAME OF FUNDING/SPONSORING ORGANIZATION 8b. OFFICE SYMBOL (If applicable)	9. PROCUREMENT INSTRUMENT IDENTIFICATION NUMBER
8c. ADDRESS (City, State and ZIP Code)	10. SOURCE OF FUNDING NOS. PROGRAM ELEMENT NO.: 63707F PROJECT NO.: 6670 TASK NO.: 15 WORK UNIT NO.: 04

11. TITLE (Include Security Classification)
Automated Cell Detection as a Mesocyclone Precursor Tool

12. PERSONAL AUTHOR(S)
Harris, F. Ian,* and Petrocchi, Pio J.

13a. TYPE OF REPORT	13b. TIME COVERED	14. DATE OF REPORT (Yr., Mo., Day)	15. PAGE COUNT
Scientific Final	FROM Oct 82 TO Sep 84	1984 October 5	32

16. SUPPLEMENTARY NOTATION
*Systems and Applied Sciences Corp.
1577 Spring Hill Road, Vienna, VA 22180

17. COSATI CODES			18. SUBJECT TERMS (Continue on reverse if necessary and identify by block number)
FIELD	GROUP	SUB. GR.	Weather radar Automated peak detection

19. ABSTRACT (Continue on reverse if necessary and identify by block number)

Automated cell detection in radar observations of convective storm complexes has been explored as a severe storm indicator. Six-dB peaks were detected in the radar reflectivity fields and their characteristics were monitored as a function of time. It was found in a severe tornadic storm that the number of cells and the average intensity of the cells had trends that appear to be characteristic of "super-cell" storms with these trends being identifiable at least 45 min before the touchdown of the first tornado and 90 min before the touchdown of a "maxi" tornado. None of these trends could be detected in a storm system that produced only a funnel cloud. This second storm did produce a tornado vortex signature. It would appear that the peak detection algorithm has the potential of extending the warning period for severe weather associated with "super-cell" and for indicating the potential of extremely severe weather. Testing has been limited and therefore these results must be considered somewhat tentative.

20. DISTRIBUTION/AVAILABILITY OF ABSTRACT UNCLASSIFIED/UNLIMITED ☒ SAME AS RPT ☐ DTIC USERS ☐	21. ABSTRACT SECURITY CLASSIFICATION Unclassified	
22a. NAME OF RESPONSIBLE INDIVIDUAL Pio J. Petrocchi	22b. TELEPHONE NUMBER (Include Area Code) (617) 861-4405	22c. OFFICE SYMBOL LYR

DD FORM 1473, 83 APR EDITION OF 1 JAN 73 IS OBSOLETE.

UNCLASSIFIED

SECURITY CLASSIFICATION OF THIS PAGE

SECURITY CLASSIFICATION OF THIS PAGE

SECURITY CLASSIFICATION OF THIS PAGE

Preface

The authors wish to thank NOAA/NSSL and the AFGL/LYR staff for their cooperation in the collection of the data used in this study. Also, we wish to thank Ralph Donaldson, Jr. and Maj. Michael Snapp for helpful comments. Harris was supported under Contract No. F19628-82-C-0023 from the Air Force Geophysics Laboratory, Hanscom AFB, Mass.

Contents

Illustrations

Illustrations

Table

Automated Cell Detection as a Mesocyclone Precursor Tool

1. INTRODUCTION

Considerable effort has been exerted to use recent advances in radar and satellite technology in short range forecasting of severe weather events. One area of considerable interest is the detection and forecasting of tornadoes. Initial efforts involved the detection of hook echoes in radar reflectivity patterns[1] as a tornado detector. However, not all tornadoes have hook echoes and not all hook echoes have associated tornadoes. Later, with the advent of Doppler radars, circulations called mesocyclones were detected in most tornadic storms[2,3] prior to and during tornadic events. Also, a characteristic signature indicative of tornadoes known as tornado vortex signature (TVS) was found. Both of these are indicative of a well-defined circulation within the storm, something that occurs well within the storm's lifecycle and are detectable with automatic real-time

---

(Received for publication 3 October 1984)

1. Fujita, T. T. (1965) Formation and steering mechanism of tornado cyclones and associated hook echoes, Mon. Wea. Rev. 93:67-78.
2. Donaldson, R. J., Jr. (1970) Vortex signature recognition by a Doppler radar, J. Appl. Meteorol. 9:661-670.
3. Burgess, D. W. (1976) Single Doppler radar vortex recognition: Part I, Mesocyclone signatures. Preprints, 17th Conf. on Radar Meteor. (Houston), Amer. Meteor. Soc., Boston, Mass. pp. 97-103.

schemes.[4,5] It has been found that initial mesocyclone detection is on average some 36 min before tornado touchdown but may be as little as a few minutes. While the mesocyclone is a tremendously useful indicator of imminent severe weather, there may be other indicators that will reduce the false alarm ratio for tornado forecasts resulting from the use of a mesocyclone detection algorithm or will at least help to extend the warning period. To this end, Donaldson and Snapp[6] examined the relative motion of echoes as a pre-mesocyclone indicator and deduced net convergence and cyclonic circulation associated with the storm that produced the Piedmont, Okla. tornado on 30 April 1978, well before the first detection of a mesocyclone. The theory here is that the intercell motion during the development phase of the storm may exhibit rotation before the mesocyclone is apparent in the radial velocity fields. Also, cell mergers are considered to be an important part of severe storm development.[7] These two studies suggest that cell behavior might well provide insight into the behavior of the storm.

In this report an objective scheme is described for the detection of cells, analyses of two storms using this detection algorithm are presented, and several parameters characterizing the cells as indicators of the storm behavior are evaluated.

2. PRE-MESOCYCLONE INDICATOR

For years people have associated features in radar reflectivity patterns with cells.[8,9] Cells are considered as fundamental elements within convective complexes, each having its own distinct lifecycle incorporating updrafts, precipitation

4. Zrnic', D.S., Hennington, L.D., and Skelton, J. (1982) Automatic Recognition of Mesocyclones from Single Doppler Radar Data, AFGL-TR-82-0291, AD A125854.

5. Wieler, J.G. (1984) Automated Real-Time Detection of Mesocyclone and Tornado Vortex Signatures, Systems and Applied Science Corp. Rpt. (in press).

6. Donaldson, R.J., Jr., and Snapp, M.R. (1983) Interstorm motion as a mesocyclone precursor. Preprints, 21st Conf. on Radar Meteor. (Edmonton), Amer. Meteor. Soc., Boston, Mass., pp. 7-10.

7. Lemon, L.R., Burgess, D.W., and Brown, R.A. (1975) Tornado production and storm sustenance. Preprints, Ninth Conf. on Severe Local Storms (Norman, Okla.), Amer. Meteor. Soc., Boston, Mass., pp. 100-104.

8. Byers, H.R. and Braham, R.R., Jr. (1949) The Thunderstorm, U.S. Dept. of Comm. Final Rpt. USDC/WB/TP-49. National Tech. Inf. Serv. PB 234 515, NTIS, Springfield, Va., 287 pp.

9. Knight, C. and Squires, P., Eds. (1983) Hailstorms of the Central High Plains, Vol. 1: The National Hail Research Experiment, Colorado Associated Univ. Press.

production, and subsequent downdraft development. When people identify cells in radar data, they are really identifying regions of enhanced values in the reflectivity factor fields. For example, see Ref. 9.

If we accept the idea that cells are in fact basic entities of convective storm systems and that significant peaks in radar measured reflectivity factor are indicators of cells, it is then possible to develop a cell detection algorithm. As is well known, though, cells come in a variety of magnitudes and sizes. For instance, a small cumulus cloud may as well be considered a cell as a giant "super-cell" storm associated with severe weather. In fact, "super-cells" must evolve from one or many little cells. Therefore, we want to be able to cover the gamut of cell magnitudes to truly characterize the behavior of the storm.

There are basically two ways to do this, namely, to key on features extending above a threshold Z value or on features extending at least some specified amount above their surrounding background. These are illustrated in Figure 1. In the threshold technique all regions above a threshold reflectivity are considered as features. For example, in Figure 1, if the threshold were 40 dBZ, two features would be identified. If 30 dBZ were the threshold, then only one peak would be picked. Bjerkaas and Forsyth[10] used this technique successfully to detect and track thunderstorms. However, as can be seen from the simple structure in Figure 1 their technique would miss the weak storms and might well miss significant structure within a storm. Since these aspects are important for our assessment of the storm evolution, this threshold technique must be considered inappropriate for our application.

In the second technique, peaks in the reflectivity factor (Z) field are found and the region around them with Z values within ΔZ of the peak value is defined as the peak. In Figure 1, the shaded regions are the one-dimensional peaks for the hypothetical curve. Crane[11] used this technique to focus on the fine scale structure within storms by detecting peaks in the reflectivity field which extended only 3 dB above the surroundings. However, Wieler et al[12] discovered that there were many problems with the significance and tracking of such features because of their large numbers, small spacing, and large relative motions.[5] It was their recommendation that larger peaks be used for such an analysis to ameliorate these problems.

---

10. Bjerkaas, C. L. and Forsyth, D. E. (1980) Operational test of a three-dimensional echo tracking program. Preprints, 19th Conf. on Radar Meteor. (Miami), Amer. Meteor. Soc., Boston, Mass., pp. 244-247.

11. Crane, R. K. (1976) Radar Detection of Thunderstorm Hazards for Air Traffic Control, Vol. 1, Storm Detection. Proj. Rpt. ATC-67-67, Vol. 1, MIT Lincoln Lab., Lexington, Mass., FAA-rd-76-52; AD A032732.

12. Wieler, J. G., Harris, F. I., and Snapp, M. R. (1982) An Evolution of an Automatic Cell Detection and Tracking Algorithm, AFGL-TR-82-0368, AD A130088.

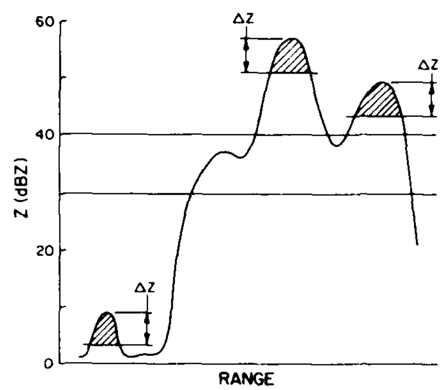

Figure 1. Schematic Depicting Structure of Acceptable Reflectivity Factor Peaks as Seen in Range

In addition, Brasunas found that the 3 dB peak detection algorithm was too computationally intensive to be seriously considered as a real-time scheme.[13]

Since the object of this effort is to characterize the storm structure as it evolves, it would appear that peak detection has the greatest potential as the basis for an algorithm. However, any algorithm that we use must require fewer computations and be more physically significant, in our opinion, than the Crane algorithm.[11] Therefore, an algorithm has been devised that incorporates those requirements.

3. ALGORITHM DESCRIPTION

As noted before, it is thought that convective cell detection and monitoring will yield insight into the status and evolution of a storm. As a consequence, a cell detection algorithm has been developed using the assumption that a cell can be identified as a feature in the reflectivity factor pattern as seen by meteorological radar. These features are defined as two-dimensional versions of the peaks noted in Figure 1. The magnitudes of these peaks should be sufficient to ensure physical significance and small enough to ensure detection of sufficient structure within the storm complex. The characteristics of these features should be reasonably well-behaved, so that one may draw realistic conclusions with regard to their behavior. The rest of this section describes an algorithm that is thought to accomplish these objectives.

13. Brasunas, J.C. (1984) A Comparison of Storm Tracking and Extrapolation Algorithm, Lincoln Lab. (M.I.T.) Rpt. ATC-124, Lincoln Lab (M.I.T.), Lexington, Mass. p. 128.

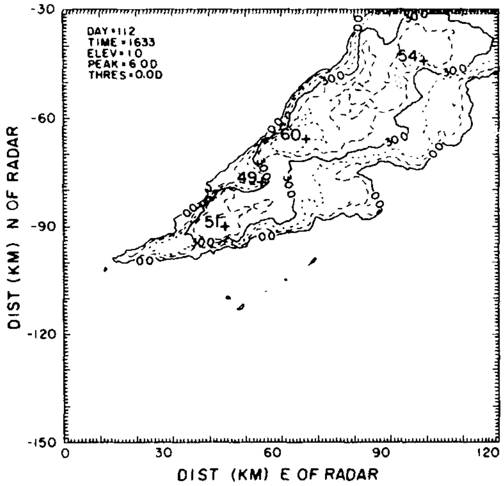

Figure 8d. Contour Plot of Z for 22 April 1978. Data were collected at Norman, Okla. at 0.7° elevation and 1633 CST. See Figure 2 for other details

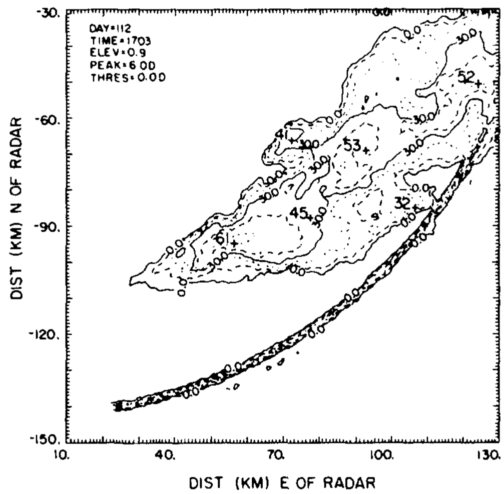

Figure 8e. Contour Plot of Z for 22 April 1978. Data were collected at Norman, Okla. at 0.7° elevation and 1703 CST. See Figure 2 for other details

towards the southeast, maintaining its line-like character. Individual cells appear to dominate at various times but none ever gets as organized as the Piedmont storm.

6.2 Temporal Continuity of Features

All of the available data collected at 0.7° elevation between 1522 CST and 1703 CST were processed for peak detection. Because of data deterioration, several scans resulted in suspect analyses in that false peaks were detected and some true features were left undetected. These scans are not considered in any further discussion. Figures 8a-8e are just a few of the successful scans processed by the peak detection algorithm. In these figures, as in Figure 2, the centroids of the detected features are depicted by the "+" symbols.

With the same procedure outlined for the previous case study, many of the detected features were tracked. Of the 83 features identified in this case, 68 (82 percent) were trackable between at least two scans with the results presented in Figure 9. Most of the detected features were associated with three main cells

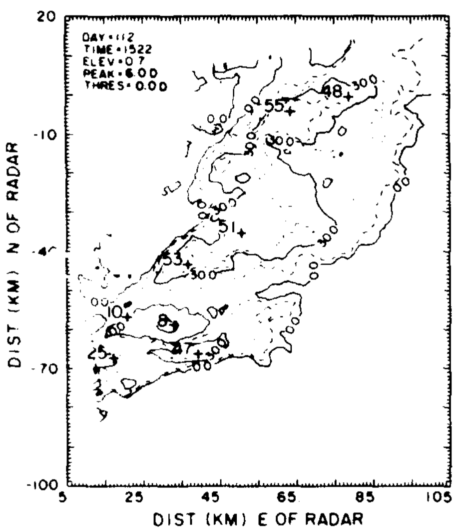

Figure 8a. Contour Plot of Z for 22 April 1978. Data were collected at Norman, Okla. at 0.7° elevation and 1522 CST. See Figure 2 for other details

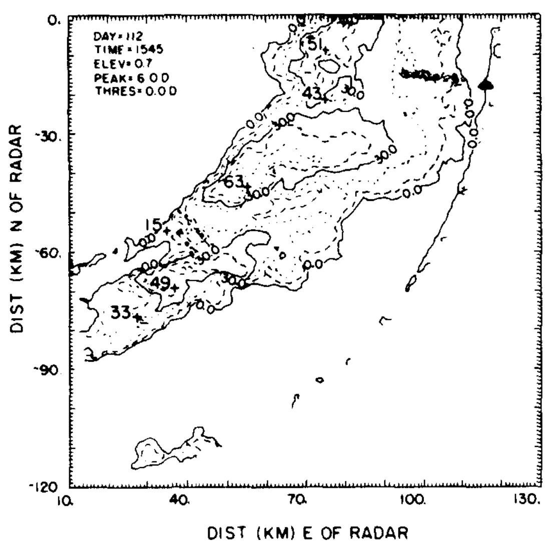

Figure 8b. Contour Plot of Z for 22 April 1978. Data were collected at Norman, Okla. at 0.7° elevation and 1545 CST. The echoes located at a constant range of 119 km here and in Figure 8c and at 140 km in Figure 8e are artifacts of the processing of the data. See Figure 2 for other details

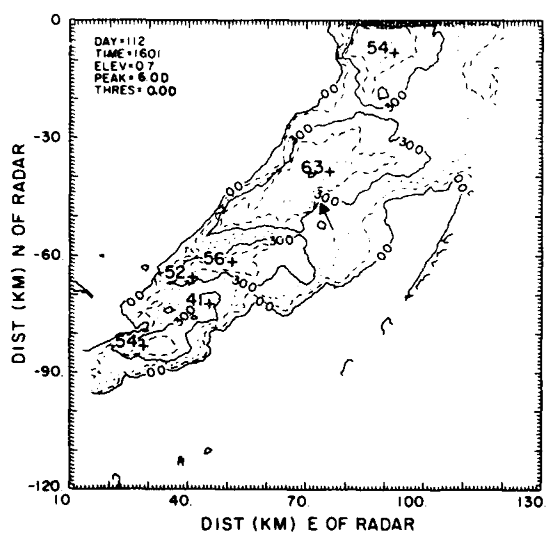

Figure 8c. Contour Plot of Z for 22 April 1978. Data were collected at Norman, Okla. at 0.7° elevation and 1601 CST. See Figure 2 for other details

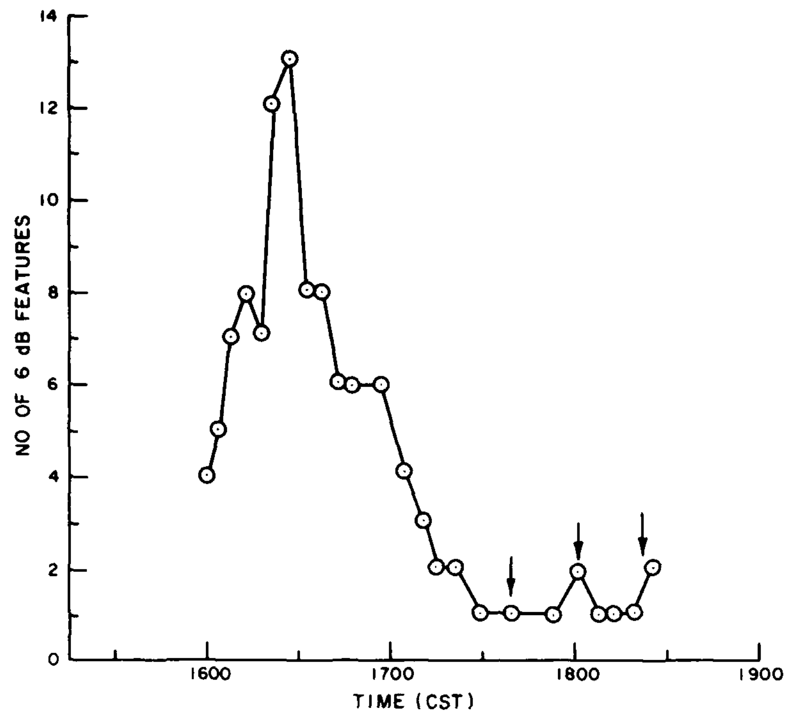

Figure 7. Number of Cells for Each Scan Plotted Against Time for 30 April 1978. Arrows above curve indicate times of tornado touchdown

the previous case study. Because the storm was further away, the 0.7° elevation scan was used for analysis.

6.1 The Storm

Data quality limitations prevented any data processing before 1522 CST, well after the initiation of echoes as is evidenced in the contour plot of the reflectivity factors at this time (Figure 8a). We see here a complex storm with several features having maximum Z's in excess of 45 dBZ. Twenty-three minutes later (Figure 8b) there are still a great many peaks, with the dominant cell appearing to be the one at (54, -43). At 1601 CST the storm is seen (Figure 8c) further to the southeast with several distinct cells organized in a line. The dominant cell appears to be the same one as 16 min earlier. It was just 7 min after this scan that the funnel cloud was observed at the location noted by the head of the arrow in this figure. During the ensuing hour (Figures 8d, 8e) the storm progressed

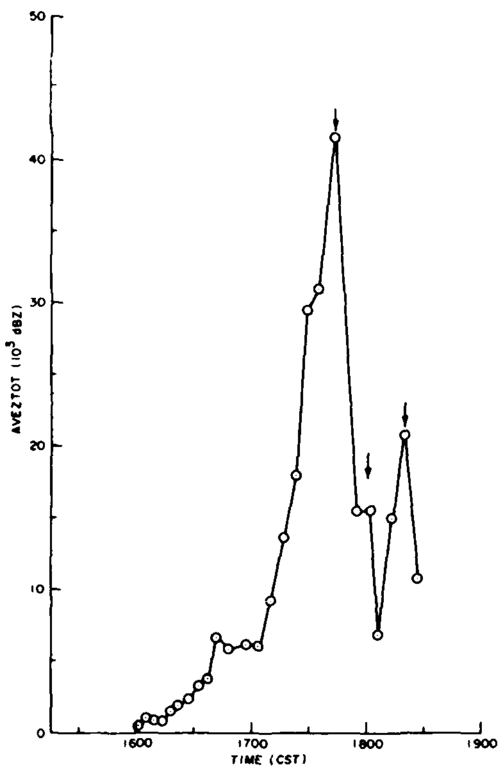

Figure 6. AVEZTOT for Each Scan Plotted Against Time for 30 April 1978. Arrows above curve indicate times of tornado touchdown

a disorganized area of more intense convection which then evolved to a very much more organized "super-cell" storm.

6. CASE STUDY - 22 APR 1978

On this date, a storm system developed southeast of Norman, Okla., evolving into a line some 150 km in length, and propagating to the southeast. Maximum reflectivity factors were observed in excess of 60 dBZ and several cells within the storm complex had marked inflow regions characteristic of intense storms. However, the only known severe weather that occurred was a funnel cloud approximately 6.5 km north of Ada, Okla., at 1608 CST. This storm was analyzed over a period from 1522 to 1703 CST, again using the NOAA/NSSL 10 cm Doppler radar at Norman. The data were collected and processed in a manner similar to that for

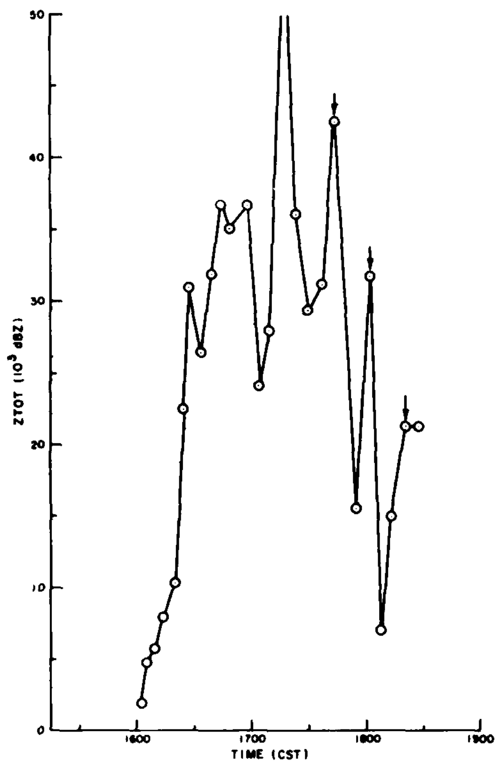

Figure 5. ZTOT for Each Scan Plotted Against Time for 30 April 1978. Arrows above curve indicate times of tornado touchdown

echo top and the descent of the echo aloft just prior to the tornado touchdown. The lowering of the storm top and the collapse of the reflectivity maximum aloft are both consistent with the increase of AVEZTOT prior to the tornado touchdown. This increase, in combination with the accompanying abrupt decrease following tornado touchdown, is a unique and striking observation. It remains to be seen if this is a unique feature of this storm or can be considered as a general characteristic of tornadic storms. From the above cited references, at least the sharp increase prior to the tornado should be a repeatable observation.

The number of cells observed at 1.5° in each of the scans is plotted in Figure 7. This plot is striking because the number of cells increases markedly from 1600 to about 1630 CST followed by a marked and steady decline in numbers until the storm essentially becomes unicellular at 1729 CST, about 10 min prior to the first tornado. This plot confirms the qualitative observation derived earlier from the contour plots that the storm evolved from an area of weak convection to

5.4 Group Characteristics of Features

To better understand the behavior of the storm, several parameters were computed for the ensemble of features at each time. As noted before, the individual reflectivity factors (in dBZ) in each feature are accumulated to form a feature ZMASS, a parameter that gives some measure of the intensity of the precipitation fallout for that feature. No attempt has been made to compensate for the resolution degradation with range in the computation of ZMASS. This could become a very important factor when storms extend over a long range but is not thought to be a significant factor in this case study. Once ZMASS for each feature is computed, a total ZMASS (ZTOT) is computed for the storm as a whole by accumulating the ZMASS's for all features. Each ZMASS is dependent upon the magnitude of the reflectivity factors as well as the total number of observations or areal extent encompassing the feature. ZTOT is dependent upon those factors plus the number of features.

Figure 5 is a plot of ZTOT versus time. In this plot, after an initial period of modest growth, there is a rapid increase in ZTOT between 1620 and 1630 from 1.0×10^4 to in excess of 3.0×10^4. For approximately 1 1/4 hr ZTOT fluctuates quite significantly but on average remains between 3 and 4×10^4. After 1740, though, there appears to be a decreasing trend in magnitude. This is during the unicellular stage noted previously and is consistent with the earlier observation that the 30 dBZ contour was decreasing in area with time (Figures 2d-2f).

AVEZTOT is plotted in Figure 6, where the ZTOT's of Figure 5 are divided by the number of features. Here, we see that for the first hour of development, the AVEZTOT increases steadily. However, in the next 30 to 40 min there is a rather rapid increase resulting in a peak in the 1741 CST scan. There is then an abrupt decrease for several scans followed by a second peak in the 1818 CST scan. While it may be considered to be a little daring to place emphasis on the second peak it should be noted that this parameter is reasonably well behaved when compared with the ZTOT curve of Figure 5. Rather amazingly, these two peaks coincide (within a minute or so) with the touchdown of the first tornado and the "maxi-tornado" associated with this storm. However, there is some support in the literature for this observation. Fujita[14] introduced the concept of the collapsing storm top as a precursor to tornado touchdown. He attributed this collapse to a decline in the updraft, allowing the precipitation to descend and interact with the developing tornado circulation. Lemon et al[7] observed the collapse of the radar

---

14. Fujita, T. T. (1973) Proposed mechanism of tornado formation from rotating thunderstorms. Preprints, Eighth Conf. on Severe Local Storms (Denver), Amer. Meteor. Soc., Boston, Mass., pp. 191-196.

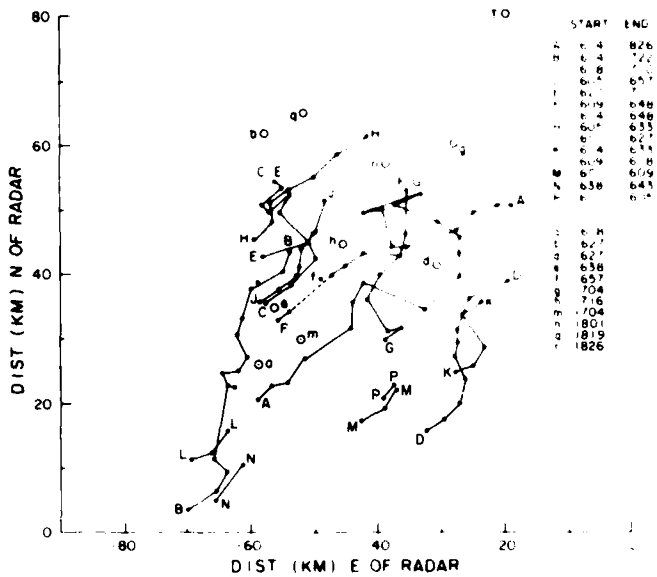

Figure 4. Tracks of All Features Detected Between 1600 and 1830 CST at 1.5° Elevation on 30 April 1978. Dashed track lines indicate tracks when there is one intervening time when the feature did not qualify as legitimate by the algorithm but was still readily apparent in the contour plots

Most of the features were trackable for at least 30 min with cells A and B (Figure 4) being tracked for 2 hr 12 min and 1 hr 8 min respectively. These two cells became dominant in terms of magnitudes of Z and of areas and ultimately merged about 1730 CST to form the unicellular storm with A appearing to be the dominant feature. By that it is meant that it appears that B merged with A and not the other way around. It should be noted that the merging of A and B is not readily apparent in Figure 4 because there we have plotted the centroids of the 6 dB peaks associated with the overall cell and just prior to the merger of the two cells their centroids were some 20 km apart. The cells, as revealed by a qualitative examination of the reflectivity factor fields, are significantly larger than the features that are detected in the algorithm. Also, at the point where B and A merged, A's track became erratic and remained erratic for about 30 min. This could be due to a reorganization of the overall internal flow, which in turn would result in a reorganization of the precipitation.

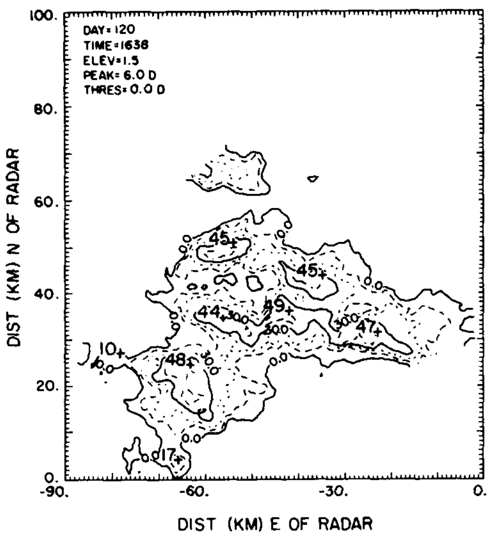

(a) 1.5° Elevation

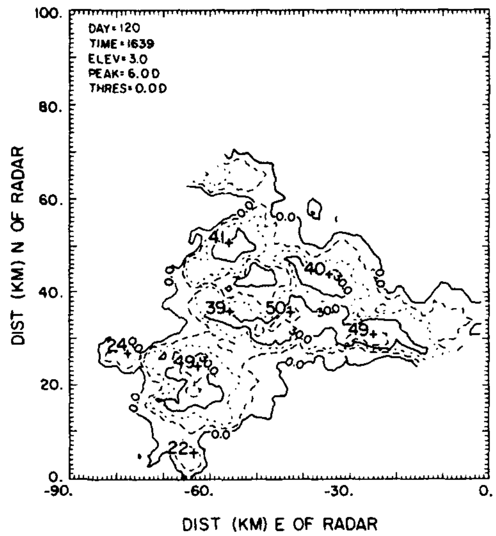

(b) 3.0° Elevation

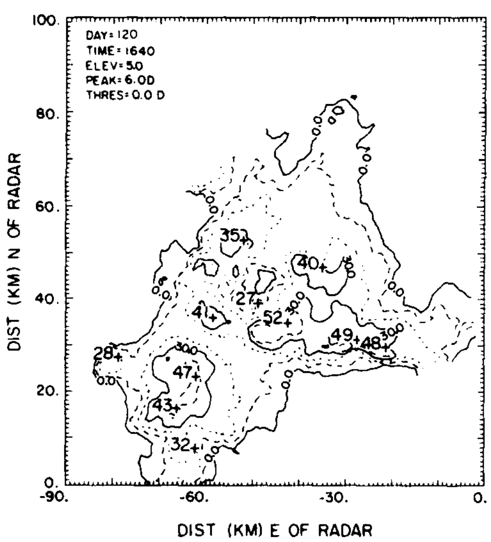

(c) 5.0° Elevation

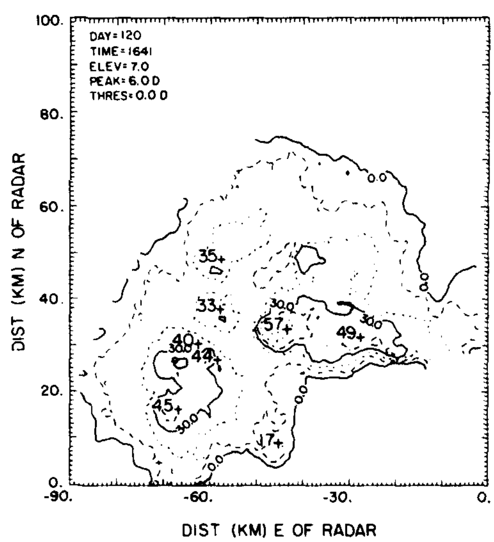

(d) 7.0° Elevation

Figure 3. Contour Plot of Reflectivity Factor for 30 April 1978. Data were collected at Norman, Okla. at 1601 CST. Contours are at 10 dBZ intervals. Locations of 6 dB peaks detected by algorithm are indicated by + signs, with peak magnitude labelled to the upper left

detection algorithm operating on data with resolution no worse than 1 km. Therefore, some differences could well be expected. Careful examination of the raw data fields verified the accuracy of the centroid computations.

Before tracking of these peaks is attempted, a close look at their behavior in space and time both as individuals and collectively is essential in order to better understand their nature. The data from the volume that started about 1638 CST were chosen for an examination of the vertical structure. Features were detected at 1.5, 3.0, 5.0, and 7.0° elevations. The reflectivity factor contour plots with associated detected peaks are plotted in Figure 3a-3d. We note that all of the peaks at 1.5° can be seen at 3 and 5° but with some dropout at 7° due to the scan being above several of the features. This high degree of vertical continuity, therefore, lends strong support to the contention that by using 6 dB peaks at 1.5°, we are detecting significant features within the storm. There are more peaks seen at higher elevations than at 1.5°. For example, note that there are a total of 11 peaks at 5° compared with 8 at 1.5°. The three additional features at (-50, 39), (-68, 16), and (-30, -31) do not have much vertical extent. The first two are seen only at 5° while the third is seen only at 5 and 7°. Therefore, one could argue that they are not significant in comparison with the other features. Quite obviously, to be thorough, one should really consider peaks at all levels, correlate them, and consider them as four-dimensional entities. However, that would be computationally much more complex and time consuming. Here, we are attempting to keep analysis simple and adaptable to real-time operations.

5.3 Temporal Continuity of Features

Features were correlated in time simply by overlaying plots similar to those in Figure 2 and using a nearest neighbor approach in combination with a visual correlation of reflectivity patterns. This subjective aspect was found to be necessary only in a few instances when echoes were too close and did not have enough temporal continuity to unambiguously correlate them with pre-existing features. Results of this tracking effort are shown in Figure 4. Of the 119 features detected in the 2 1/2 hr of observations only 11 were not associable with at least one other feature in an adjacent scan. However, all of these 11 were qualitatively associated with structures at adjacent heights and scans that were not strong enough to be identified as 6 dB peaks. This high degree of continuity suggests that the size of the peaks being detected is close to optimum, at least for this storm.

The features generally tracked towards the northeast with some tendency for cyclonic curvature to the track for those cells on the east side. However, this tendency is not strong enough to be a very useful characteristic.

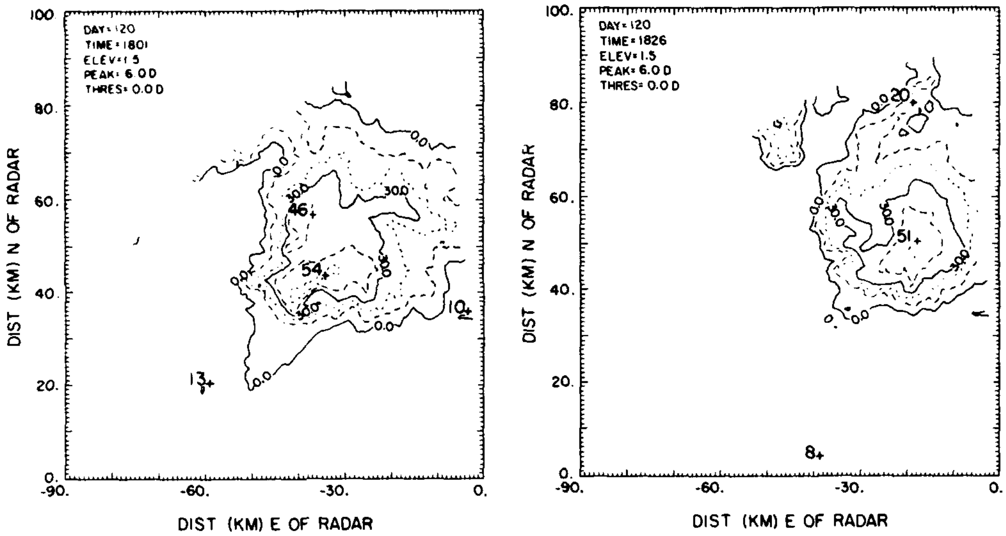

(e) 1801 CST (f) 1826 CST

Figure 2. Contour Plot of Reflectivity Factor for 30 April 1978. Data were collected at Norman, Okla. at 1.5° elevation. Contours are at 10 dBZ intervals. Locations of 6 dB peaks detected by algorithm are indicated by + signs, with peak magnitude labelled to the upper left (Contd)

now has two distinct reflectivity maxima. The more southern feature, however, appears to be the dominant one, both in terms of magnitude and area. The area within the 30 dBZ contour has decreased quite significantly during this time and appears to reduce even further by 1819 CST (Figure 2f), approximately the time of the maxi-tornado. At this time the storm is again unicellular.

5.2 Peak Detection

All of the 1.5° elevation scans available between 1600 and 1830 CST were processed for peak detection. The centroid positions of each of the detected peaks are depicted in Figures 2a-2f as "+" with the magnitude of the maximum Z shown to the upper left of the "+". It should be noted that in these figures the centroid is not always where one might necessarily expect it to be from the shape of the reflectivity contours. For example, the 54 dBZ (-35,44) centroid position at 1801 CST (Figure 2e) is not within the 50 dBZ contour. However, this is a dBZ-weighted centroid position and is located between the two 50 dBZ contours, in a region where Z does not fall below 48 dBZ. Also, one needs to keep in mind that the contour plots in Figures 2a-2f are contours of interpolated data, where the interpolation filter radius is 1 km and the grid spacing is 1 km. Therefore, we are comparing data smoothed over 2 km with results of analyses by the peak

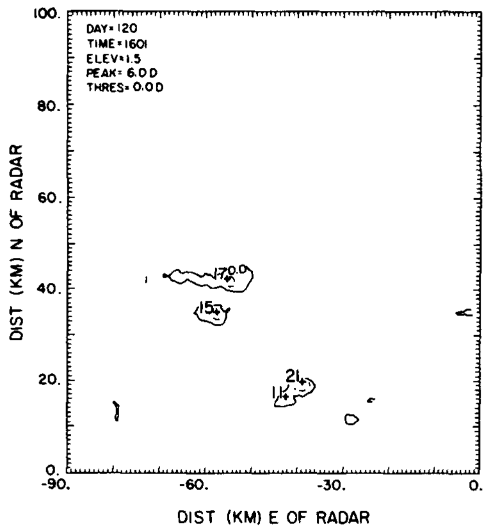

(a) 1601 CST

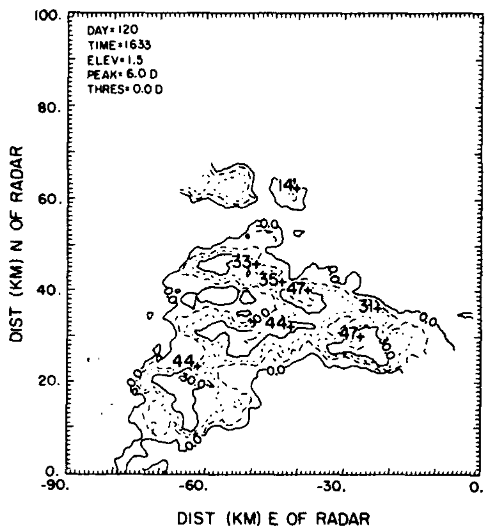

(b) 1633 CST

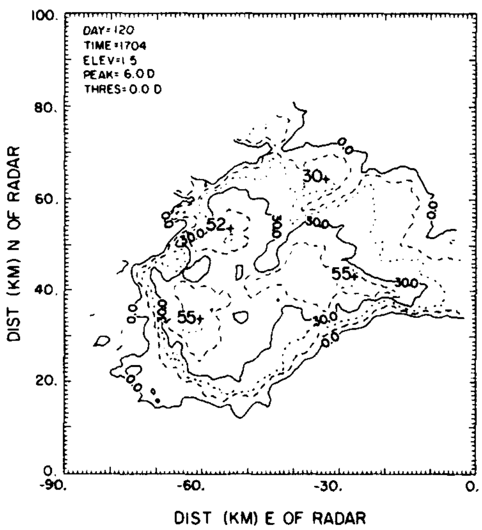

(c) 1704 CST

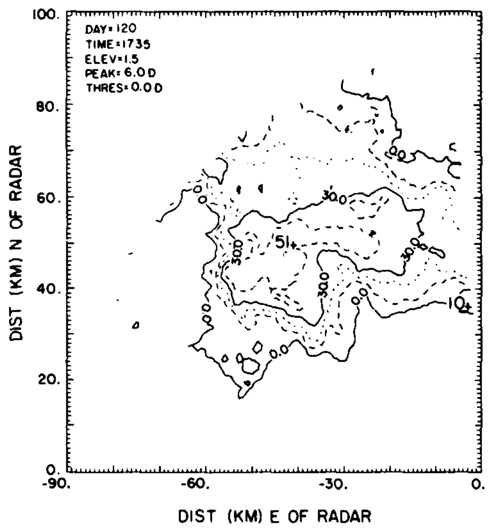

(d) 1735 CST

Figure 2. Contour Plot of Reflectivity Factor for 30 April 1978. Data were collected at Norman, Okla. at 1.5° elevation. Contours are at 10 dBZ intervals. Locations of 6 dB peaks detected by algorithm are indicated by + signs, with peak magnitude labelled to the upper left

where a feature was not properly identified even after the feature correlation. These scans were not included in this study.

5. CASE STUDY - 30 APR 1978

On 30 Apr 1978, a storm developed some 30 to 70 km west of Norman, Okla., the site of the radar used for this study. The first echoes appeared about 1600 CST. These cells intensified and evolved into a classical "super-cell" that resulted in a small tornado about 1740 CST, followed by three small tornadoes at 1800 and a "maxi-tornado" at 1820 CST at Piedmont, Okla. Radar data were collected throughout this period at Norman, Okla., with the 10 cm Doppler radar belonging to the National Severe Storms Laboratory, National Oceanic and Atmospheric Administration (NOAA/NSSL). The data were input into and processed by the Air Force Geophysics Laboratory radar data acquisition system. Data were collected continuously while the antenna made complete 360° scans at elevation angles of 0.7, 1.5, 3.0, 5.0, and 7.0° approximately every 7 min. Data were analyzed for the 1.5° scans because they were high enough to be relatively clutter free and low enough so that effects of height differences in range are minimized in any interpretation of results. Also, while echoes tend to be first seen aloft at heights of 7 km or greater (see for example Ref. 9), there may well be many more features at higher levels, features that are weaker and perhaps more transient. Examination of the low level data will tend to focus more on the "significant" cells, although one can obviously lose features due to merging of precipitation patterns.

5.1 The Storm

At 1601 CST there were four small echoes located some 50 km west of the radar site. Maximum reflectivity in each echo at this height ranged from 10 to 21 dBZ (Figure 2a). There is no apparent organization to the echoes at this time. By 1633 CST (Figure 2b) there are more cells, but they are no longer entirely separate entities; instead, they are joined into what might be thought of as a loose collection where no one echo appears to be dominant. By 1704 CST (Figure 2c) the structure of the storm has become much more simplified, taking on more of the character of a multicellular storm. Thirty minutes later (Figure 2d), the echo is even more simplified in appearance, with dBZ values peaking at 51 dBZ. The structure at this time is much more characteristic of a "super-cell", with the inflow region being denoted by the weak-echo region or reflectivity notch on the southern edge of the storm and the highest reflectivity in a horseshoe around it. At 1801 CST (Figure 2e) the storm still has its notch on the south flank but

Table 1. Algorithm Output

FEATURE	
	Peak Reflectivity Location in relation to Radar No. of Beams in Which Feature Occurred ZMASS Location in relation to Center of Mass Nearest Neighbor Distance
STORM	
	ZTOT Location of Center of Mass Average ZMASS Total No. of Peaks Mean Closest Neighbor Distance

4. ALGORITHM PARAMETER SELECTION

The size of the peaks being detected is, in a way, the most critical aspect of this peak detection scheme. One wishes to detect cells, that is, features that have temporal and spatial continuity. But one also wants to detect entities that will still characterize the internal structure of the storms. Crane's approach[11] could be adopted, wherein one chooses a small value (for example, 3 dB) for the peak and relies on temporal and spatial continuity for acceptance. The problem found with that approach is that because the number of peaks observed is so great, false vertical and even temporal continuity relationships can be derived.[12] The approach used here is to try much larger peaks, namely 6 dB. It was found that 6 dB peak detection appeared to identify most of the significant structure within the storm while 10 dB peak detection resulted in a significant portion of the internal structure being ignored. The temporal and spatial continuity of the 6 dB peaks will be discussed later (in the case studies).

In the nearest neighbor tests for peak association it was found necessary to apply a maximum inter-peak distance in order to accept a correlation. Through an iterative approach it was determined that a maximum separation of 15 range gates (4.5 km) captured most of the features. This allowed features to be identified within complex storms with a minimum of false associations. Also, with the correlation for truncated features outlined earlier, most remaining loose ends due to complex structures tended to be resolved. There were two or three scans

The first task is to detect cells using a peak detection scheme. The goal is to process the data as it is received and to keep the analysis as simple as possible. Therefore, the current analysis is only two-dimensional and has no temporal correlation scheme. The data are processed radial by radial by averaging over each series of three points and then looking for all peaks (Z_p) regardless of magnitude within a range- and azimuth-limited region. These peaks are then scanned and only those that extend some prescribed value (ΔZ) above their surroundings are kept. All future references to peaks will be to that portion of the reflectivity factor curve plotted against range that extends on either side of the Z_p until the values of Z fall below $Z_p - \Delta Z$, that is, peaks are the shaded portions under the curve in Figure 1. Range centroid positions are computed for each peak and the Z's within that peak are accumulated. For both of these calculations there must be at least three points along the beam within the peak, that is, there must be at least three contiguous points that have $Z > Z_p - \Delta Z$.

These peaks in range are stored for the remainder of the scan. Once the scan is processed, the peaks are correlated in azimuth using a nearest neighbor criterion and stored as features. A particular peak must be (1) the closest one to the feature and (2) on an adjacent radial and within 15 range gates of the last occurrence of a feature for association to occur. Once all peaks are identified with features, all features are scanned to determine whether they are complete in azimuth (that is, the peaks are at least ΔZ above their surroundings or are truncated) and are appropriately labeled. Centroid positions and accumulated reflectivity factors (ZMASS) are computed for each feature. Truncated features are then checked against the others to determine if they can be correlated to form complete features or added on to existing ones. Here we relax the correlation distances to 10 km to account for large complex systems, but require the features being correlated to be nearest neighbors and the peak reflectivities at the correlating azimuths to be within ΔZ of each other. This prevents most spurious correlations. Finally, only those features that are complete and are found in three or more azimuths are used for the later analyses.

Several computations are made for each scan. These are listed in Table 1.

Data for each elevation are processed independently. There is no vertical correlation nor is there any temporal correlation conducted in the processing software. However, these aspects are discussed later.

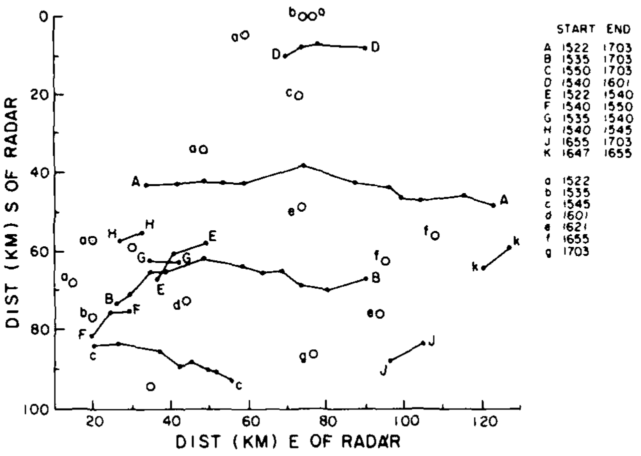

Figure 9. Tracks of All Features Detected Between 1522 and 1703 CST at 0.7° Elevation on 22 April 1978

as can be seen by their tracks in Figure 9. In general, all of the cells tracked in an easterly direction. There was no major convergence of cells as was seen 8 days later. Some of the single time features in the southwest flank of the storm were mergers with the two southern long-lived storms. However, there does not appear to be a significant effect on the overall storm severity due to this merger.

6.3 Group Characteristics of Features

Figure 10 is a plot of ZTOT for all of the features detected in each scan as a function of time. As for the Piedmont storm, this parameter yields little insight into the overall behavior of the storm. Average magnitudes are less than those in Figure 5 despite the overall larger area and overall greater number of features in this storm. The presentation of AVEZTOT in Figure 11 (ZTOT/no. of features) shows very little change during the entire period of observation, with no distinct character before the funnel cloud as seen in Figure 6. Also, the number of cells versus time (Figure 12) plot shows none of the structure seen in the corresponding plot for the Piedmont storm. Just prior to the funnel cloud (1608 CST) there was a decrease in the numbers from 8 to 6, but this does not appear to be significant. In general, the temporal characteristics seen in all of these parameters as being associated with tornado development in the previous case are not at all apparent prior to the funnel cloud observation of this case.

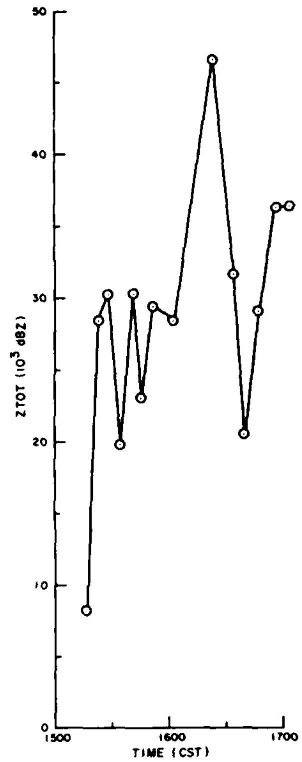

Figure 10. ZTOT vs Time for 22 April 1978

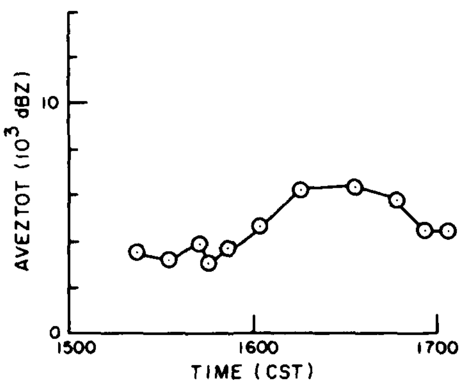

Figure 11. AVEZTOT vs Time for 22 April 1978

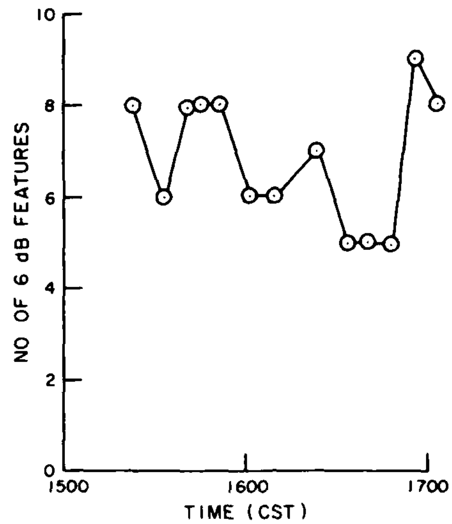

Figure 12. No. of Cells
vs Time for 22 April 1978

7. DISCUSSION

Two quite different storm types were studied to assess the efficacy of automatic detection of storm peaks as indicators of imminent mesocyclone/tornado development. For a storm producing several tornadoes, one of which was a "maxi-tornado", there were several clear indicators. The number of cells increased markedly during the first 1/2 hr and then decreased sharply during the following hour as it evolved into a classic "super-cell" storm. This period was also characterized by a marked increase in the average accumulated Z over all features (AVEZTOT). The decrease in AVEZTOT about the time of the first tornado is entirely consistent with the previous observations of cloud top collapse about 10 min prior to tornado touchdown and with the observation of the collapse of the bounded weak echo region also seen just prior to touchdown. The fact that the storm on April 22 shows none of these characteristics suggests that it was not able to undergo the same degree of organization as the Piedmont storm. Therefore, it may well be possible to assess the development of TVS signatures as to severity of any associated vortex through an examination of the degree of storm organization as revealed by the examination of cell behavior. Also, it should be noted that the first detection of a mesocyclone on April 30 occurred about

1650 CST. If one could recognize the characteristics of Figures 6 and 7 as early as 1635 CST then we may be able to advance the warning time by another 15 min.

Quite obviously, any conclusions drawn from only two cases must be considered tentative. However, it is well known that the most severe weather tends to be associated with "super-cells" and squall lines. Squall lines, per se, have not been addressed here, and there must be some question of the application of this algorithm to that situation. However, for the "super-cell" cases, the reasoning for detection appears to be sound.

It would appear that the algorithm as presented here results in a reasonable detector of the development of "super-cells", and hence the development of extremely severe weather. The increase of organization evidenced by the decrease of numbers of cells and the increase in storm "severity" as indicated by the rapid increase in AVEZTOT, are consistent with prior observations. It is perceived that the use of this or a similar algorithm along with a mesocyclone/TVS algorithm may yield advance warning of the potential of extremely severe tornadic activity associated with a particular storm system. The indicators do not appear to be very sensitive to marginal severe weather. Therefore they are unlikely to be useful as anything other than a "super-cell" predictor. However, this in itself could be useful. Also, we feel that the potential of peak detection as an analysis and forecast tool has not been totally realized. For too long people have been constrained by the limitation of the size of the peak that was being sought. It is felt that we have demonstrated here that by relaxing this peak magnitude condition we can increase our understanding of the development of a particular storm system.

References

1. Fujita, T. T. (1965) Formation and steering mechanism of tornado cyclones and associated hook echoes, Mon. Wea. Rev. 93:67-78.
2. Donaldson, R.J., Jr. (1970) Vortex signature recognition by a Doppler radar, J. Appl. Meteorol. 9:661-670.
3. Burgess, D.W. (1976) Single Doppler radar vortex recognition: Part I, Mesocyclone signatures. Preprints, 17th Conf. on Radar Meteor. (Houston), Amer. Meteor. Soc., Boston, Mass. pp. 97-103.
4. Zrnic', D.S., Hennington, L.D., and Skelton, J. (1982) Automatic Recognition of Mesocyclones from Single Doppler Radar Data, AFGL-TR-82-0291, AD A125854.
5. Wieler, J.G. (1984) Automated Real-Time Detection of Mesocyclone and Tornado Vortex Signatures, Systems and Applied Science Corp. Rpt. AFGL-TR-84-0282, Contract F19628-82-C-0023.
6. Donaldson, R.J., Jr., and Snapp, M.R. (1983) Interstorm motion as a mesocyclone precursor. Preprints, 21st Conf. on Radar Meteor. (Edmonton), Amer. Meteor. Soc., Boston, Mass., pp. 7-10.
7. Lemon, L.R., Burgess, D.W., and Brown, R.A. (1975) Tornado production and storm sustenance. Preprints, Ninth Conf. on Severe Local Storms (Norman, Okla.), Amer. Meteor. Soc., Boston, Mass., pp. 100-104.
8. Byers, H.R. and Braham, R.R., Jr. (1949) The Thunderstorm, U.S. Dept. of Comm. Final Rpt. USDC/WB/TP-49. National Tech. Inf. Serv. PB 234 515, NTIS, Springfield, Va., 287 pp.
9. Knight, C. and Squires, P., Eds. (1983) Hailstorms of the Central High Plains, Vol. 1: The National Hail Research Experiment, Colorado Associated Univer. Press.
10. Bjerkaas, C.L. and Forsyth, D.E. (1980) Operational test of a three-dimensional echo tracking program. Preprints, 19th Conf. on Radar Meteor. (Miami), Amer. Meteor. Soc., Boston, Mass., pp. 244-247.

11. Crane, R.K. (1976) Radar Detection of Thunderstorm Hazards for Air Traffic Control, Vol. 1, Storm Detection. Proj. Rpt. ATC-67-67, Vol. 1, MIT Lincoln Lab., Lexington, Mass., FAA-rd-76-52; AD A032732.

12. Wieler, J.G., Harris, F.I., and Snapp, M.R. (1982) An Evolution of an Automatic Cell Detection and Tracking Algorithm, AFGL-TR-82-0368, AD A130088.

13. Brasunas, J.C. (1984) A Comparison of Storm Tracking and Extrapolation Algorithm, Lincoln Lab. (M.I.T.) Rpt. ATC-124, Lincoln Lab (M.I.T.), Lexington, Mass. p. 128.

14. Fujita, T.T. (1973) Proposed mechanism of tornado formation from rotating thunderstorms. Preprints, Eighth Conf. on Severe Local Storms (Denver), Amer. Meteor. Soc., Boston, Mass., pp. 191-196.

END

FILMED

7-85

DTIC